ACS OMEGA

Open Access

http://pubs.acs.org/journal/acsodf

Article

Enhanced Electrochemical Detection of Nonelectroactive Compounds Based on Surface Supramolecular Interactions on Chevron-like Graphene Nanoribbons Modified through Click Chemistry

Rut Martínez-Moro, Luis Vázquez, María Pérez, María del Pozo, Manuel Vilas-Varela, Jesús Castro-Esteban, M. Dolores Petit-Domínguez, Elena Casero,* and Carmen Quintana*

Cite This: *ACS Omega* 2024, 9, 39242−39252

Read Online

ACCESS | Metrics & More | Article Recommendations | Supporting Information

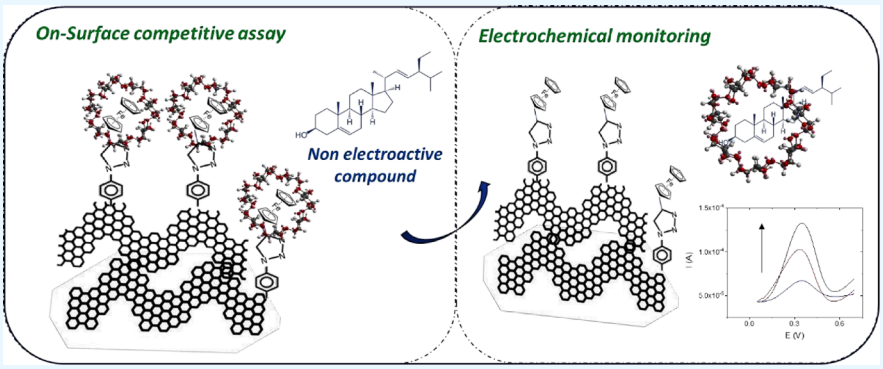

ABSTRACT: In this study, we have developed a nanostructured electrochemical sensor based on modified graphene nanoribbons tailored for the analysis of nonelectroactive compounds via a surface competitive assay. Stigmasterol, a nonelectroactive phytosterol, was selected as a representative case. Chevron-like graphene nanoribbons, chemically synthesized, were immobilized onto glassy carbon electrodes and covalently functionalized to allow the on-surface formation of a supramolecular complex. To this end, the nanoribbons were first modified through a diazotization process by electrochemical reduction of a 4-azidoaniline diazonium salt, leaving the electrode surface with azide groups exposed to solution. Next, the incorporation of a ferrocene group, as a redox probe, was carried out by a click chemistry reaction between ethynylferrocene and these azide groups. Finally, the recognition event leads to the formation of a supramolecular complex between ferrocene and a macrocyclic receptor on the electrode surface. To this end, the receptors cucurbit[7]uril, cucurbit[8]uril, and β-cyclodextrin were evaluated, with the better results obtained with β-cyclodextrin. Atomic force microscopy and scanning electron microscopy measurements were performed for the morphological characterization of the resulting electrochemical platform surface. The ability of β-cyclodextrin to form an inclusion complex with ferrocene or with stigmasterol allows to perform a competitive assay, which translates into the decrease and recovery of the ferrocene electrochemical signal. For stigmasterol determination, a linear concentration range between 200 and 750 μM and a detection limit of 60 μM were obtained, with relative errors and relative standard deviations less than 7.1 and 9.8%, respectively.

1. INTRODUCTION

Carbon-based nanomaterials with different dimensionalities, and consequently different properties,[1,2] have been widely used, either alone[3−6] or in combination with metal complexes and oxides,[7−14] as electrode modifiers in electrochemical sensors, leading to enhanced performances. Among carbon nanomaterials, graphene nanoribbon (GNR) applications have been scarcely explored.[15] GNRs are composed of strings of sp^2 carbon atoms and exhibit improved and novel properties compared to graphene. These properties can be tailored by controlling their width and edge structure, prompting researchers to control GNR synthesis at the atomic level.[16] Synthesis methods of GNRs can be classified into two main groups: bottom-up and top-down. Unzipping single- and multiwalled carbon nanotubes, employing metal catalysis or oxidation exfoliation methods, is among the most commonly used top-down approaches. However, these methods typically

Received: July 18, 2024
Accepted: August 2, 2024
Published: September 4, 2024

Scheme 1. Steps of the Sensor Construction and Competitive Assay for Stigmasterol Determination

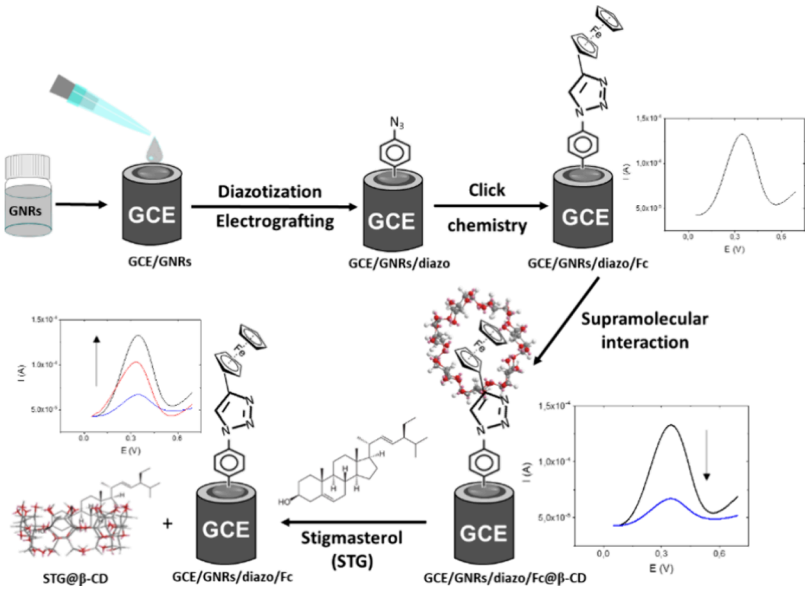

result in GNRs with widths exceeding 10 nm and offer limited control over their edge structure.[17] Bottom-up synthesis involves assembling molecular building blocks to form GNRs via on-surface or solution synthesis.[15,16] In this case, the resulting GNRs exhibit a more precise edge structure and higher yields, making these methodologies preferable.

GNRs can be functionalized by noncovalent and covalent methods in order to enhance their applicability. Noncovalent functionalization can be achieved by the adsorption of molecules on the GNRs surface, but this method presents as major drawback that these molecules can be easily detached from the surface. Covalent functionalization of GNRs improves their chemical reactivity and electronic properties, making it the most controllable functionalization method.[18,19] Electrode surfaces can be modified with diazonium salts, via the electrografting method, allowing further covalent reactions to adapt the functional groups to the final application of the sensors.[15,20−22] In this electrografting approach, diazonium salts are electrochemically reduced to generate reactive radicals that bind covalently to the electrode surface, forming a strong covalent bond between the electrode and the diazonium compound. Furthermore, these diazonium compounds can undergo 1,3-cycloaddition click chemistry reactions to attach other molecules or functional groups. For example, this can include the incorporation of electrochemically active species such as ferrocene,[22] which modulates the electrochemical activity of the sensor improving its performance. The employment of these strategies over GNRs enables their covalent functionalization, thereby overcoming the application limitations associated with these nanomaterials.

Host−guest interactions via supramolecular receptors improve the performance of electrochemical sensors due to their enhanced selectivity.[23] Macrocyclic receptors used for this purpose have been extensively studied in the past decade, with cyclodextrins being the most employed molecules. These cyclic oligosaccharides consist of six, seven, or eight D-glucose units bonded via α-1,4- glycosidic linkages, forming a nonsymmetric toroidal structure with a hydrophilic outer surface and a lipophilic central cavity of varying sizes.[24−26] These structural characteristics make cyclodextrins a highly selective family of macrocyclic receptors, depending the recognition of a given analyte not only on the size of the analyte but also on its solubility properties, enabling them to form inclusion complexes with a wide range of molecules. β-cyclodextrin (β-CD), composed of seven D-glucose units, is the most commonly used due to its abundance in nature. Moreover, since the beginning of this century, other macromolecular receptors, known as cucurbit[n]urils (CB[n]s), have emerged as a powerful alternative to cyclodextrins in various applications, including sensor construction.[27] CB[n]s (n= 5−10) are pumpkin-shaped cyclic polymeric synthetic compounds composed of n glycoluryl units. They feature two symmetrical portals delimited by carbonyl oxygen atoms, allowing guests to be accommodated within the hydrophobic cavity.[28]

High levels of cholesterol in blood lead to cardiovascular diseases;[29] thereby, there has been plenty of research focused on human cholesterol in comparison to phytosterols, despite the beneficial properties of this family of compounds, such as reducing blood cholesterol levels[30] or their potential anticancer properties.[31] Phytosterols are molecules with a structure similar to animal cholesterol, which can be found in vegetables. Their study has been carried out over the years with good results, using various techniques, mainly gas chromatography (GC) and high-performance liquid chromatography (HPLC) coupled with detectors such as a mass spectrometer (MS). Other research approaches include Fourier transform infrared spectroscopy (FTIR), colorimetric assays, and UV−vis spectroscopy. The choice of technique for analysis depends largely on the nature of the sample.[32−39] However, these techniques have several disadvantages, primarily related to expensive equipment, the need for skilled personnel to handle the analysis, and the tedious methods required for sample preparation before analysis. In this regard, electrochemical techniques represent a promising alternative since they are more cost-effective, require less complex equipment, and are suitable for conducting *in situ* analysis. Numerous articles demonstrate these advantages, showing the high versatility and variety of novel electrochemical sensors that enable the development of platforms specifically designed for different

https://doi.org/10.1021/acsomega.4c06639
ACS Omega 2024, 9, 39242−39252

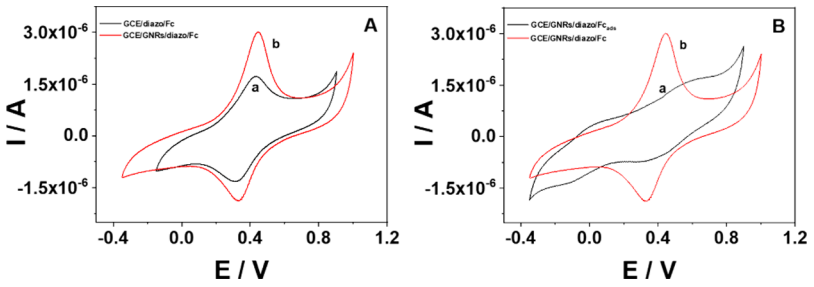

Figure 1. (A) Cyclic voltammetry response of (a) GCE/diazo/Fc and (b) GCE/GNRs/diazo/Fc sensors. (B) Cyclic voltammograms recorded with (a) GCE/GNRs/diazo/Fc_{ads} and (b) GCE/GNRs/diazo/Fc. 0.1 M $NaClO_4$. Scan rate = 100 mV/s.

analytes. However, the number of studies focused on the electrochemical determination of phytosterols is limited due to the lack of electroactivity of these compounds. In this sense, we have selected one member of this family, stigmasterol (STG), as a representative phytosterol to demonstrate the ability of our method for determining this kind of compound. The method, enabling quantification of analytes with no electrochemical response, is based on combining the use of macrocyclic receptors with the modification of electrodes with moieties presenting redox activity. The receptors tend to diminish the electrochemical signal from the moieties immobilized on the electrode by forming a supramolecular complex. Then, in the presence of the analyte, competition is established between the moiety and the analyte for the receptor cavity. If the receptor's affinity for the analyte is higher than for the electrochemical moiety, the receptor will be released into the solution to form a complex with the analyte, thereby recovering the electrochemical signal.

Here, we present a novel electrochemical sensor based on modified GNRs for the analysis of stigmasterol, a nonelectroactive phytosterol, using a surface competitive assay. To achieve this, (i) GNRs were drop-cast onto a glassy carbon electrode (GCE) surface and subsequently modified by electrografting with a diazonium salt (GCE/GNRs/diazo). (ii) A 1,3-cycloaddition click reaction was then performed to attach a ferrocene group (Fc), generating a redox signal (GCE/GNRs/diazo/Fc). (iii) This signal was inhibited when a supramolecular complex with β-cyclodextrin was formed (GCE/GNRs/diazo/Fc@β-CD). (iv) The competitive assay between the analyte, stigmasterol, and ferrocene for the β-cyclodextrin cavity allowed the recovery of the ferrocene signal, which is the basis of the application of the sensor.

2. RESULTS AND DISCUSSION

The main goal of the electrode modification was to construct a supramolecular complex onto the electrode surface with an electroactive guest. Scheme 1 shows the different steps followed to prepare the nanostructured electrode surface. First, the electrode is modified with a GNR suspension (GCE/GNRs) and left to dry. Afterward, the electrode is immersed in a diazonium salt solution, previously formed by the reaction between 4-azidoaniline and sodium nitrite, in which it is electrografted on the GNR surface (GCE/GNRs/diazo). In the third step, the azide group attached to the electrode reacts with the alkyne group of the ethynylferrocene through a "click" reaction (GCE/GNRs/diazo/Fc). The incorporation of this ferrocene moiety on the electrode surface can be easily followed by electrochemical measurements. Ferrocene was selected as a electrochemical probe as it is a well-known guest of different macrocyclic receptors. Once the supramolecular receptor (CB[7], CB[8], or β-CD) was incorporated, leading to GCE/GNRs/diazo/Fc@CB[n] and GCE/GNRs/diazo/Fc@β-CD sensors, the electrochemical signal of the ferrocene was diminished. Finally, after a competitive assay with the nonelectroactive analyte, stigmasterol, the increase of the electrochemical signal will allow the analyte determination.

2.1. Effect of the Electrode Nanostructuration and Click Chemistry on the Electrochemical Signal. We studied the effects of both electrode nanostructuration with GNRs and the use of click chemistry for immobilizing the ferrocene moiety on the electrochemical signal of GCE/GNRs/diazo/Fc. In Figure 1A, the effect of performing the electrografting over a GNR-modified GCE instead of onto a bare GCE is depicted. It can be observed that this step is highly efficient if it is performed over GNRs. Clearly, we got a higher Fc amount on the electrode with GNRs (GCE/GNRs/diazo, voltammogram b) than without GNRs (GCE/diazo, voltammogram a), as can be deduced from the higher oxidation and reduction signals recorded for the first mentioned system.

These results suggest that the presence of GNRs on the electrode surface enhances its performance, likely due to increased electron charge transfer and a larger effective surface area. To validate these points, we compared the interfacial electrochemical properties and electroactive surface areas of the GCE and GCE/GNRs systems.

To evaluate the increase in the electrochemical active surface area (ECSA) due to the presence of GNRs on the electrode surface, we recorded cyclic voltammograms using hydroquinone (HQ) as the redox probe for GCE/GNRs and GCE systems at 100 mV/s (Figure S1A). The electrochemical surface area was determined from the Randles−Sevcik equation:

$$I_{pa} = (2.6910^5)n^{3/2}AD^{1/2}v^{1/2}C \quad (1)$$

where I_{pa} is the anodic peak current measured in Figure S1A, n is the number of electrons (n = 2), A is the electrochemical surface area, D is the hydroquinone diffusion coefficient (2.3×10^{-5} cm^2 s^{-1}), v is the scan rate (100 mV/s), and C is the concentration of the hydroquinone (2.5 mM). Under these conditions, an increase of around 21% in the electroactive surface was obtained for the GCE/GNRs system. This increase in area can explain the higher efficiency of the electrografting process when performed on an electrode modified with GNRs. Moreover, the interfacial electrochemical properties were evaluated using electrochemical impedance spectroscopy (EIS) employing 2.5 mM HQ in a 0.1 M phosphate buffer pH 7.0 (see Figure S1B). The Nyquist plot for the bare electrode displays a semicircle followed by a linear segment. The semicircle corresponds to the electron transfer-limited

https://doi.org/10.1021/acsomega.4c06639
ACS Omega 2024, 9, 39242−39252

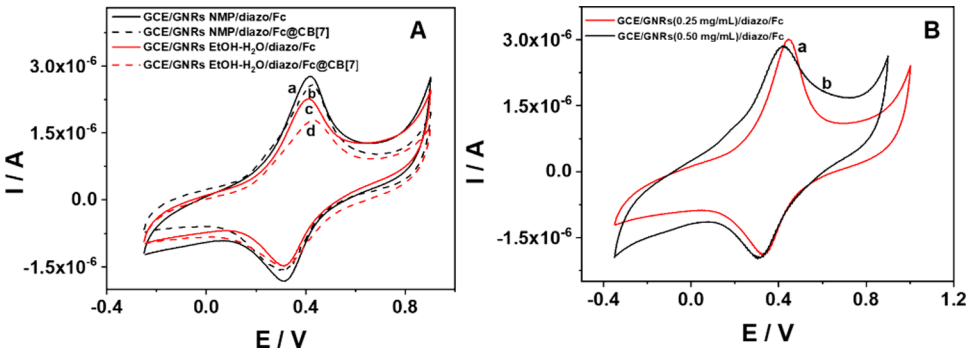

Figure 2. (A) Cyclic voltammetric response of (a) GCE/GNRs-NMP/diazo/Fc, (b) GCE/GNRs-NMP/diazo/Fc@CB[7], (c) GCE/GNRs-EtOH-H_2O/diazo/Fc, and (d) GCE/GNRs-EtOH-H_2O/diazo/Fc@CB[7] sensors. (B) Cyclic voltammetric response of (a) GCE/GNRs/diazo/Fc (0.25 mg/mL GNRs) and (b) GCE/GNRs/diazo/Fc (0.50 mg/mL GNRs) sensors with 0.1 M $NaClO_4$. Scan rate = 100 mV/s.

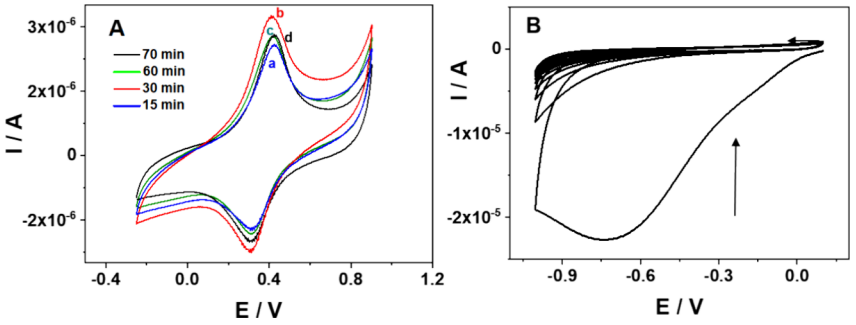

Figure 3. (A) Influence of the reaction time on the diazonium salt formation: (a) 15, (b) 30, (c) 60, and (d) 70 min. HCl 0.5 M under a N_2 atmosphere. T = 4 °C. (B) Influence of the number of CV scans on the diazonium salt electroinjection. Scan rate = 200 mV/s.

process, with its diameter indicating the electron transfer resistance at the electrode interface. The linear segment at low frequencies represents the diffusion process. In contrast, the Nyquist plot for the GCE/GNRs shows a straight line, indicating a significant improvement in charge transfer with a diffusion-limited transport process being observed.

Next, the effect of immobilizing the Fc group through a click chemistry reaction was studied. As shown in Figure 1B, the immobilization of Fc without performing the click chemistry reaction (GCE/GNRs/diazo/Fc_{ads}, voltammogram a), where Fc is adsorbed but not covalently attached, led to a small and poor response. This is in contrast to the reversible redox response recorded with an electrode surface, where Fc groups have been covalently attached in a more controlled way (GCE/GNRs/diazo/Fc, voltammogram b).

In order to confirm the reversible behavior for the GCE/GNRs/diazo/Fc system, we have performed a Laviron analysis, consisting of recording cyclic voltammograms in $NaClO_4$ 0.1 M at different scan rates (v) and plotting $E^{\circ\prime}-E_p$ versus ln v (see Figure S2). In the Laviron equations,

$$E_{pc} = E^{0'} - \frac{RT}{\alpha nF}\ln\frac{\alpha nFv}{RTk_{ET}} \quad (2)$$

$$E_{pa} = E^{0'} - \frac{RT}{(1-\alpha)nF}\ln\frac{(1-\alpha)nFv}{RTk_{ET}} \quad (3)$$

E_p is either the cathodic or the anodic peak potential, $E^{\circ\prime}$ is the formal potential, α is the electron transfer coefficient, n is the number of electrons (n = 1), k_{ET} is the electron transfer rate constant, and R, F, and T have the usual meaning. From the slope of the linear part of the plot, a α value of 0.51 is obtained, which is in agreement with the reversible process. In conclusion, although Fc groups can be adsorbed on the GNRs in a nonspecific way, the electrografting step is essential for the subsequent "click chemistry" reaction through which we incorporate the redox probe (Fc) to the electrode.

2.2. Optimization of the Sensor Construction. Once we have demonstrated the suitability of nanostructuring the electrode surface with GNRs and covalently attaching Fc through click chemistry, we optimized each step of the sensor construction.

2.2.1. GNR Concentration and Solvent. As the first step in sensor construction involves the modification of the GCE with GNRs, it is critical to obtain a homogeneous and well-dispersed initial suspension of this nanomaterial. The literature reveals the use of *N*-methylpyrrolidone (NMP) as one of the best solvents for GNR dispersion.[40] In addition to this solvent, we evaluated, as a greener option, a mixture of EtOH/H_2O (1:1, v/v). The influence of the solvent employed to prepare the GNR suspension was studied by following the ferrocene voltammetric response obtained for sensors prepared with each GNR suspension (GCE/GNRs-NMP/diazo/Fc and GCE/GNRs-EtOH-H_2O/diazo/Fc). From the results (Figure 2A), a slightly higher Fc oxidation current was recorded with the GNRs dispersed in NMP (votammogram a, I_p = 2.7 μA) than that obtained in EtOH/H_2O (votammogram c, I_p = 2.3 μA). These results seem to indicate that modification of the electrode with GNRs in NMP allows the adsorption of a greater amount of Fc groups. However, when the GCE/GNRs/diazo/Fc system is subjected to supramolecular complexation, better results are obtained using EtOH/H_2O, as reveals the decrease in Fc signal after the supramolecular reaction (voltammogram d). This decrease is less pronounced in the case of using GNRs in NMP (voltammogram b). In

https://doi.org/10.1021/acsomega.4c06639
ACS Omega 2024, 9, 39242−39252

addition, NMP results are difficult to eliminate, leading to a worse nanostructuration of the electrode surface. Likewise, the greater amounts of Fc would lead to an excessive proximity between them, which hinders, to a certain extent, the formation of the supramolecular complex. Moreover, the mixture EtOH/H_2O presents the advantage of getting dried much faster than NMP. Therefore, EtOH/H_2O (1:1, v/v) was selected as a solvent.

Next, the amount of GNRs employed to prepare the suspension in EtOH/H_2O was also optimized. As can be observed in Figure 2B, a lower capacitive current and better-defined Fc signals are obtained with 0.25 mg/mL GNR suspensions with respect to those with a higher concentration. Consequently, the next experiments were performed employing 0.25 mg/mL GNR suspensions in an EtOH/H_2O (1:1, v/v) mixture.

2.2.2. Diazotization Process. The optimization of the diazotization step was performed on the basis of different procedures previously reported.[41−43] We studied both the time required for achieving the reaction between 4-azidoaniline and $NaNO_2$ and the optimum number of cyclic voltammetric scans to generate and covalently attach the aryl radical of the diazonium salt onto the surface.

First, 4-azidoaniline and $NaNO_2$ were let to react for 15, 30, 60, or 70 min, and as before, the Fc electrochemical signal after the click reaction was used to test the effect of this variable. Figure 3A shows that Fc current increases while increasing the reaction time from 15 to 30 min, but longer times do not lead to higher Fc signals. Therefore, we kept 30 min for further experiments.

Next, we scanned the potential between 0.1 and −1.0 V during 10 cycles at 200 mV/s (see Figure 3B). The decrease of the reduction wave at −0.7 V with successive cycles confirms the electrochemical grafting of the diazonium salt on the surface. From the results, it is established that 10 scans are enough to ensure that the electrografting process is complete, and no more salt can be electroinjected.

2.2.3. Click Chemistry Reaction. Different parameters involved in the "click chemistry" reaction (i.e., ethynyl-Fc concentration, the ratio EtOH/H_2O employed as a solvent, and the incubation time) were studied. Figure 4A shows the influence of the ethynyl-Fc concentration when it was varied between 0.3 and 1.0 mM. As the 0.3 mM concentration allowed the highest Fc current, it was selected for the rest of the experiments. In order to confirm this point, we also tested 0.2 mM, observing a slight decrease compared to 0.3 mM (data not shown).

Due to the different solubilities of the reagents involved in the click reaction, the relation of both solvents (EtOH and water) was tested as depicted in Figure 4B. The best response was obtained when the reaction was performed with an EtOH/H_2O 4:1 (v/v) ratio.

Finally, the incubation time for this click reaction was also studied by varying the time during which the GCE/GNRs/diazo dispersion was immersed in the ethynyl-Fc solution in the presence of the reducing agent (ascorbic acid) and the catalyst (Cu I). As depicted in Figure 4C, the number of Fc groups attached on the electrode surface increases until 18 h as can be concluded from the increase of the oxidation Fc current recorded in the experiments, diminishing for higher times.

For a clear overview of the sensor preparation procedure, the optimized parameters and optimal conditions for obtaining a highly sensitive sensor are summarized in Table S1.

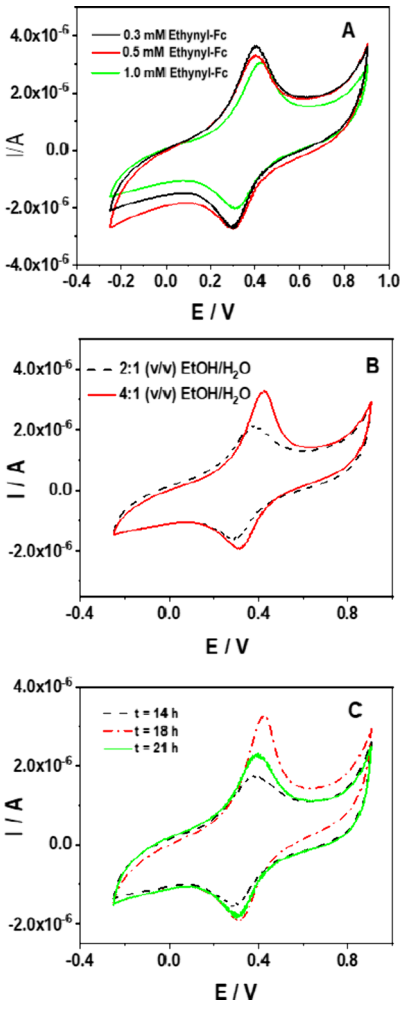

Figure 4. GCE/GNRs/diazo/Fc response for sensors prepared employing (A) different ethynyl-Fc concentrationss, (B) different ratios of the EtOH/H_2O solvent, and (C) different incubation times of the GCE/GNRs/diazo electrode in the 1.0 mM ethynyl-Fc solution. Scan rate = 100 mV/s.

2.2.4. Supramolecular Complex Formation. The last step in electrode surface nanostructuration is the on-surface supramolecular complex formation. To this end, different macrocyclic receptors, i.e., CB[7], CB[8], and β-CD, were assayed as hosts of the Fc moiety. The experiments were performed as follows: the GCE/GNRs/diazo/Fc sensor was immersed into the corresponding aqueous receptor solution, and the Fc oxidation current was monitored, at regular intervals of time from 0 to 24 h. To better monitor the signal changes and increase the sensitivity of the method, we employed differential pulse voltammetry for these and further experiments.

Figure 5A summarizes the results of such a set of assays. As observed, the results are similar, irrespective of the macrocyclic used as all three are good Fc hosts. In all cases, the Fc signal decreases quickly in the presence of the receptor and remains constant after 7−8 h. Both CB[8] and β-CD lead to the minimum Fc signal, which is the most favorable situation for the competitive assay. As β-CD is cheaper and quite better soluble in water than CB[8], it was employed for the sensor preparation and for the competitive assay with stigmasterol. Figure 5B displays the DPV measurements after the supra-

https://doi.org/10.1021/acsomega.4c06639
ACS Omega 2024, 9, 39242−39252

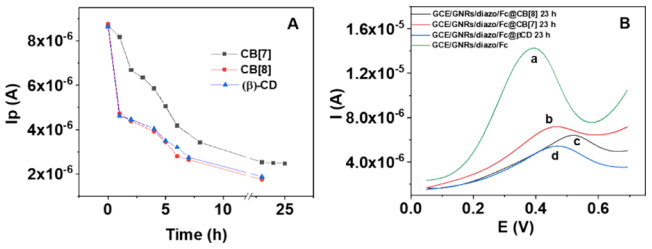

Figure 5. (A) Ip recorded with the GCE/GNRs/diazo/Fc after different incubation times in CB[7] (black line), CB[8] (red line), and β-CD (blue line) solutions. (B) Differential pulse voltammograms of GCE/GNRs/diazo/Fc before (voltammogram a) and after 23 h of incubation in CB[7] (voltammogram b), CB[8] (voltammogram c), and β-CD (voltammogram d).

molecular complexation event (23 h of immersion time) for the three receptors employed. As no I_p variation was produced for immersion times longer than 18 h, this value was selected for the rest of the experiments.

Finally, the charge transfer behavior of GCE/GNRs/diazo/Fc before and after being complexed with β-CD was studied by CV and EIS using $NaClO_4$ 0.1 M as an electrolyte. As can be seen in the Nyquist plot displayed in Figure S3B, the GCE/GNRs/diazo/Fc shows a linear segment with a slope higher than one, characteristic of adsorbed species. As evidenced by both the diminution of the response in the CV (Figure S3A) and the semicircle observed in the Nyquist plot (Figure S3B) for the GCE/GNRs/diazo/Fc@β-CD system, the encapsulation of the Fc in a hydrophobic environment hinders the charge transfer.

2.3. Morphological Characterization of the Building Steps in the Sensor Construction. We have characterized by scanning electron microscopy (SEM) the morphology of the electrode surface after each building step of the sensor (Figure S4). In Figure S4A is displayed a low-magnification image of the drop-cast GNR solution on the GCE surface. A wide size distribution of the GNRs features is obtained, with size from a few nanometers up to ~10 μm. The darkest structures, which display perimeters with well-defined angles, likely correspond to thin GNR layers. This is supported by the atomic force microscopy (AFM) image of the same sample shown in Figure S5, which displays topographical and phase-contrast images on a given area of the sample. The GNR flake is clearly observed in the phase-contrast image. In contrast, in the topographical image, this structure is not apparent, which is due, likely, to its extreme thinness as well as to the GCE surface roughness.

Figure S4B–D also shows characteristic high- (insets) and low-magnification images of the different building steps (GCE/GNRs/diazo, GCE/GNRs/diazo/Fc, and GCE/GNRs/diazo/Fc@β-CD, respectively). The images show that no substantial changes are induced along the building process, as the wide size distribution and morphology of the GNRs structures are similar. It is worth noting that the organic material deposited in these steps is difficult to detect by SEM due to the relatively high electron energy employed in the measurements.

Because of this lack of contrast by SEM imaging, we have studied these samples by AFM. Due to the wide GNR size distribution, we have to look for small GNRs flakes that can be reliably measured. Figure 6A shows a large scan of the GCE/GNRs/diazo/Fc sample. In the top right corner, a thick (>350 nm) GNR structure is observed. Its surface looks rather flat. In order to better asses the surface morphology of the flakes, the inset of Figure 6A shows a detail of one flake (placed at the right half of the inset) together with the surface profile along the white solid line. The flake is just 3 nm thick, and its surface shows corrugations below the nanometer.

It should be noted that similar features were found for the GCE/GNRs/diazo sample. In this system, we performed force curve studies on top of the modified GNR flakes with the aim to assess the diazo layer thickness formed on the surface. These curves display the cantilever deflection (vertical axis) as the tip approaches the surface from the right of the horizontal axis and contacts it, and the tip further presses on the surface. We have made a similar analysis, with the same tip, on the GCE and GCE/GNRs surfaces as the stiff references. The results are plotted in Figure 6B. The curves present a horizontal region at the right, indicating that the tip is far from the surface and there is no interaction between them (i.e., there is no cantilever deflection). Then, moving to the left, the deflection goes downward due to the van der Waals tip–sample interaction, indicating that the tip is close to the surface. Then, the deflection begins to increase sharply because the tip touches the surface and the repulsive interaction operates. For the GCE and GCE/GNRs surfaces from the contact point to the left, the behavior is a straight line, indicating that both surfaces are stiffer than the cantilever. In contrast, for the GCE/GNRs/diazo surface, once the tip contacts the surface, there is,

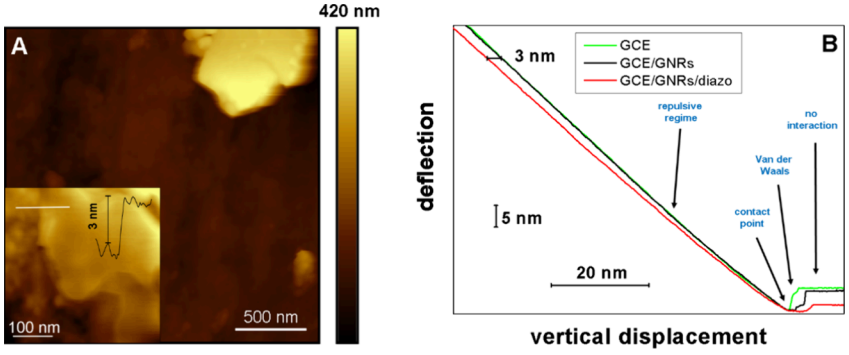

Figure 6. (A) AFM image of the GCE/GNRs/diazo/Fc system, showing a large and thick GNR structure at the top right. Inset: high-magnification image of a 3 nm-thick GNR flake whose profile along the white solid line is also depicted. (B) Force curves obtained with the same cantilever on GCE (green), GCE/GNRs (black), and GCE/GNRs/diazo (red). The thickness of the diazo layer is 3 nm as indicated. In the plot are indicated the different tip–sample interaction regimes, namely, no interaction, attractive van der Waals, contact point, and repulsive region.

https://doi.org/10.1021/acsomega.4c06639
ACS Omega 2024, 9, 39242–39252

initially, a certain curved region before reaching the linear dependence with the same slope as that observed for GCE and GCE/GNRs. The curved region corresponds to the tip sampling the soft diazo layer, whereas once the tip has gone through this layer, the linear regime is attained, as the tip is already interacting with the stiffer GCE or GCE/GNRs. This fact makes that the constant slope regime of the force curve for the GCE/GNRs/diazo shifts leftward with respect to that of GCE and GCE/GNRs. This shift of 3 nm is the thickness of the soft diazo layer. This value agrees with previous reports of multilayer deposition.[41,44−46]

Figure 7A shows a characteristic AFM image of the general morphology of the GCE/GNRs/diazo/Fc@β-CD system. The

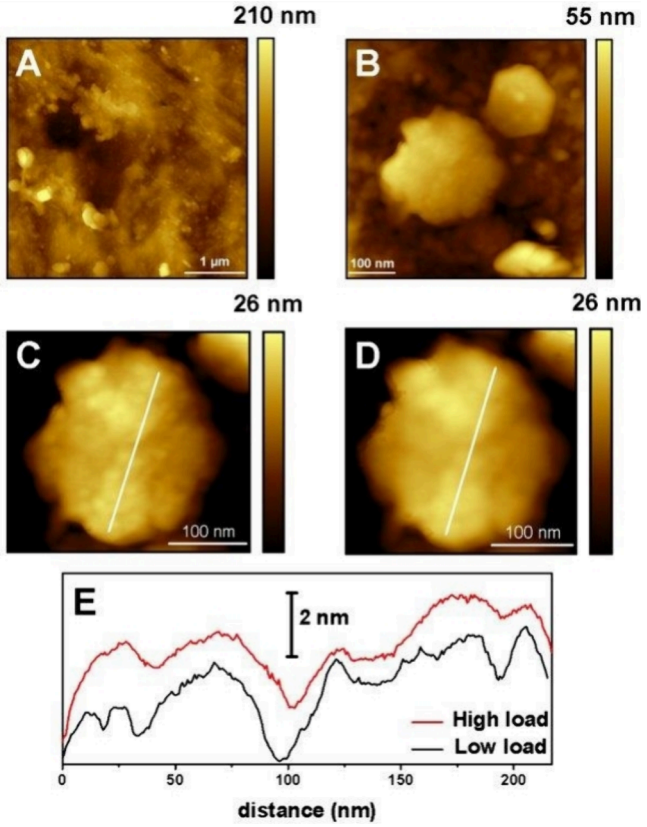

Figure 7. AFM images of the CGE/GNRs/diazo/Fc@β-CD system. (A) 4 × 4 μm^2; (B) 500 × 500 nm^2 image showing two flakes. (C,D) 300 × 300 nm^2 images of a single flake obtained at low (C) and high (D) loads. (E) Surface profiles along the white solid lines depicted in (C) and (D).

background shows the surface of the polished GC electrode, in which some parallel lines are observed, which are due to the initial treatment. Scattered on the surface are found relatively flat flakes (see the bottom part and the bottom left part of the image). They present different tiltings with respect to the GCE surface. Figure 7B shows a close view of two of these flakes observed at the bottom of Figure 7A.

Figure 7B suggests that the surface of the flakes presents a certain structure in contrast to those of the previous systems. This fact is confirmed when a single flake is imaged (Figure 7C). Clearly, this figure shows that the flake surface is covered by a layer of globular structures, which was absent when the flake was modified with diazo and Fc (see the inset in Figure 6A). Accordingly, the surface roughness of the flake increases with respect to that of the bare GNR flakes (around 0.5 nm, see ref 41) up to 2.2 nm). Now, corrugations up to 4−5 nm high can be measured on top of the flakes (Figure 7E), while in the GCE/GNRs/diazo/Fc, they were below 1 nm. Here, it is important to stress the fact that the load applied by the tip during the imaging process can affect the visualized surface. This is exemplified by Figure 7C,D that corresponds to the same flake imaged at low (Figure 7C) and high forces (Figure 7D). When a low force is employed, the globular structures are clearer. However, when a higher force is applied, these structures become blurred and wider. This is due to their soft character that allows their deformation and distortion under the tip load. Accordingly, the surface roughness of the same flake reduces to 1.4 nm. The effect of the applied force on the morphology is better appreciated in Figure 7E where the surface profiles along the same locations of the flake for both load conditions are plotted. That one obtained at low force shows a richer morphology with higher roughness and lateral resolution. These results evidence the soft nature of this layer. These structures can be ascribed, due to the small size of the ferrocene, to β-CD. The size of the globular imaged structures, in the 6−8 nm range, is larger than that of one β-CD molecule. This is explained by the tendency of CDs to aggregate leading to larger structures.[47] Finally, it should be noted that when the surface is imaged again at a low tip load, the globular structures recover their initial appearance, which indicates that the aggregate was deformed elastically and not plastically.

2.4. Evaluation of the GCE/GNRs/diazo/Fc@β-CD Sensor Response toward Stigmasterol Concentration. Finally, we evaluated the ability of the dispersion to electrochemically respond to nonelectroactive compounds. In this case, stigmasterol was selected as the analyte for the competitive assay. First, we studied the incubation time required for recovery of the Fc signal. To this end, the GCE/GNRs/diazo/Fc@β-CD sensor was submerged in a 750 μM STG solution at various times. Figure 8A shows how, from the response of the GCE/GNRs/diazo/Fc@β-CD dispersion (voltammogram a), the increase of the incubation time led to the progressive recovery (voltammograms c, d, and e) of the initial GCE/GNRs/diazo/Fc signal (voltammogram b). From the results, 30 min was enough for the competitive assay to take place and, therefore, selected to evaluate the response of the dispersion toward different STG concentrations.

In these conditions, we found that the recovery of ferrocene signal increased linearly with stigmasterol concentration in the 200−750 μM concentration range, according to the equation $(I/I_0)\ 100 = (0.07 \pm 0.01)\ [STG]\ \mu M + (35 \pm 6)$, $r = 0.97$ (Figure 8B), where I_0 and I are the intensity obtained with GCE/GNRs/diazo/Fc@β-CD before and after incubating in increasing concentrations of stigmasterol, respectively. From the results, detection and quantification limits of 60 and 198 μM were obtained, respectively.

The accuracy and precision (in terms of repeatability and reproducibility) of the proposed methodology were evaluated at different stigmasterol concentration levels in the linear range. As shown in Table 1, relative errors (Er %) lower than 7.1% and relative standard deviation (RSD %) values lower than 7.1 and 9.8% for repeatability and reproducibility were obtained, respectively. Recoveries, higher than 92.9% are also included in the table. Finally, the high stability of the sensor over time (82% of the initial ferrocene signal is maintained over 30 days) confirms the strong ferrocene covalent grafting on the electrode.

https://doi.org/10.1021/acsomega.4c06639
ACS Omega 2024, 9, 39242−39252

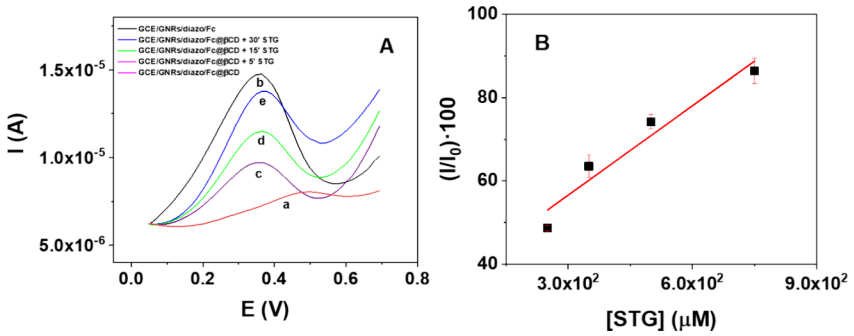

Figure 8. (A) Differential pulse voltammograms recorded with GCE/GNRs/diazo/Fc@β-CD before (a) and after a given incubation time (c,d,e) in a solution of 0.1 M $HClO_4$ containing [STG] = 750 μM. The response obtained for GCE/GNRs/diazo/Fc is also included (b). (B) Recovery of the Fc signal after incubating GCE/GNRs/diazo/Fc@β-CD for 30 min in increasing concentrations of stigmasterol (250, 350, 500, and 750 μM). Each concentration was measured three times (n = 3).

Table 1. Er % (n= 3), RSD % (n = 3), and Recovery Values for the Developed Method at Different STG Concentrations

[STG] (μM)	Er (%)	repeatability RSD (%)	reproducibility RSD (%)	recovery (%)
350	7.1	5.9	4.3	92.9
500	7.0	4.5	2.3	93.0
750	3.5	7.1	9.8	96.5

As mentioned above, only a scarce number of electrochemical sensors for stigmasterol determination can be found in the literature due to its lack of electroactivity. In particular, to the best of our knowledge, only one study involving the employment of β-cyclodextrins in the sensor construction has been published.[32] In contrast, other methods requiring more complex instrumentation, such as gas chromatography (GC) and high-performance liquid chromatography (HPLC) coupled with various detectors, have been employed to this end.[33,35−39] In Table S2, a comparison of the linear concentration range, the detection limits, and the reproducibility obtained with different methods is presented. As can be observed, our developed method presents a comparable linear concentration range and reproducibility to others, with the advantages of being more cost-effective, requiring less complex equipment and not needing sample preparation. Although a higher detection limit is obtained, it is sufficient for achieving phytosterol determination, considering the typical concentration of these compounds in real samples.

Finally, we selected two compounds with similar size and polarity characteristics, amantadine and cholesterol, to be evaluated as potential interferences in the determination of stigmasterol. For this, increasing concentrations of the interferent were added to a solution containing 250 μM STG. To be considered an interferent, the compound had to produce a change in the initial signal equal to or greater than 10%. For amantadine, no interference is produced up to a concentration 5-fold higher than that of STG. Under these conditions, a variation of 7% occurs. In the case of cholesterol, interference is produced at a 1:1 ratio of cholesterol-to-STG concentration.

3. CONCLUSIONS

In this work, we have demonstrated the role that both click chemistry and supramolecular chemistry can play in the electrochemical sensor field for applications related to the determination of nonelectrochemically active analytes. The preparation of a nanostructured electrode surface based on chevron-like graphene nanoribbons functionalized by electrografting of a diazonium salt allowed us the covalent attachment of a ferrocene moiety, which plays a double role: providing a redox signal and acting as a host for the receptor leading to an on-surface supramolecular complex. Among the different macromolecular receptors assayed to this end, namely, CB[7], CB[8], and β-CD, the latter one showed the best performance for the complete sensor design (GCE/GNRs/diazo/Fc@β-CD). AFM images of the CGE/GNRs/diazo/Fc@β-CD surface reveal flakes ascribed to GNRs covered by a layer of globular structures of aggregated β-CDs. These aggregates were elastically deformed by the tip. The proposed strategy, based on a competitive assay, allowed us to develop an electrochemical method for detecting the nonelectroactive compound stigmasterol at the 60 μM level with very good accuracy and precision (Er < 7.1% and reproducibility as RSD < 9.8%, respectively). The developed methodology offers a promising alternative to other conventional methods due to its cost-effectiveness, potential for miniaturization enabling *in situ* analysis, and the requirement for less complex equipment.

4. EXPERIMENTAL SECTION

4.1. Reagents. Phenanthrene-9,10-quinone, 1,3-diphenylacetone, *N*-bromosuccinimide (NBS), diphenylacetylene, bis-(1,5-cyclooctadiene) nickel(0) (Ni $(COD)_2$), iron trichloride, sodium perchlorate, cholesterol, amantadine, 4-azidoaniline, ascorbic acid, ethynylferrocene (ethynyl-Fc), cucurbit[n]urils (n = 7 and 8, denoted as CB[7] and CB[8], respectively), and β-cyclodextrin (β-CD) were obtained from Sigma-Aldrich. Ethanol absolute (EtOH) (99%), *N*-methylpyrrolidone (NMP), copper sulfate pentahydrate, and sodium nitrite were purchased from Scharlab S.L. All reagents were of analytical grade and used without further purification. Ultrapure water was obtained from a Milli-Q system of Merck Millipore.

4.2. Apparatuses. The electrochemical measurements were carried out with an Autolab PGSTAT 302N potentiostat employing Gpes software (both from Metrohm Autolab) equipped with a frequency response analyzer (FRAII).

Atomic force microscopy (AFM) data were obtained with a Nanoscope IIIa system (Veeco) operating in dynamic mode (intermittent contact mode). Contact mode was discarded because of the soft character of some of the materials involved in sensor construction. Accordingly, silicon cantilevers (Bruker) with a relatively low force constant (1−5 N/m) were employed with the aim to image these soft surfaces, such

https://doi.org/10.1021/acsomega.4c06639
ACS Omega 2024, 9, 39242−39252

as the cyclodextrin structures. In this sense, low free amplitudes were used in order to minimize the tip−sample interaction and, thus, to reduce the extent of the distortion of the soft structures during the imaging process. The images were composed of 512 pixels × 512 pixels. The scan rate was ∼1 Hz. The nominal cantilever radius was ∼8 nm.

We also performed force curve studies on top of the GNR structures on some systems. In this case, we employed an Agilent 5500 (PicoPlus) microscope that operates in the intermittent contact mode but that allows to perform force curves on selected spots of the image. We want to note that we mainly addressed these studies to relatively small flakes since when larger, rougher ones were visualized, the tip became damaged to some extent that avoided reliably imaging the flake surface.

SEM measurements were done with NOVA NANOSEM 230 equipment (FEI) and using a low-voltage and high-contrast detector (vCD). The landing electron beam energy was 3−4 keV.

A Bandelin Sonopuls ultrasonic probe was used for the preparation of the graphene nanoribbon suspension.

4.3. Procedures. *4.3.1. Chevron-like Graphene Nanoribbon Synthesis.* GNRs were synthesized according to previously reported protocols.[15,17,41] Briefly described, after bromination of phenanthrene-9,10-quinone with *n*-bromosuccinimide, a condensation step with 1,3-diphenylacetone, and a reaction with diphenylacetylene, a monomer was obtained. In the next step, GNRs were obtained by Ni $(COD)_2$-promoted polymerization of this monomer followed by $FeCl_3$-promoted cyclodehydrogenation. Finally, a 0.25 mg/mL GNR suspension was prepared in EtOH/H_2O 1:1 (v/v) and treated with an ultrasonic probe during 2 min with a 70% amplitude.

4.3.2. Electrochemical Sensor Preparation. The GCE/GNRs/diazo/Fc@*β*-CD-modified surface was prepared by successive modifications steps, as described below.

4.3.2.1. GCE/GNRs Preparation. The GCE surface was polished with an alumina powder (0.3 *μ*m), sonicated alternatively in water/ethanol for 3 min, and dried with a N_2 stream. Next, it was modified by drop casting with 10 *μ*L of the GNR suspension and dried in an oven at 70 °C during 1 h. The morphological and structural characterization of GCE/GNRs was reported in previous works.[15,41]

4.3.2.2. GCE/GNRs/diazo/Fc: Electrografting and "Click Chemistry" Reaction. The functionalization of the GCE/GNRs with a ferrocene group was carried out by electrografting of a diazonium salt followed by a click chemistry reaction[42] with ethynylferrocene. For this click reaction to occur, the presence of an azide group exposed to ethynylferrocene is necessary. Therefore, the diazonium salt was prepared from diazotization of azidoaniline as follows: 250 *μ*L of sodium nitrite (0.2 M) was added to a N_2-purged 4-azidoaniline solution (5.9 mM) prepared in HCl 0.5 M (10 mL) and thermostated at 4 °C. This mixture was let to react during 30 min under a nitrogen atmosphere. Next, the electrografting on the GCE/GNRs surface was produced by 10 successive cyclic potential scans from 0.1 to −1.0 V at 200 mV/s in the diazonium salt solution. This procedure led to covalent attachment of the corresponding aryl radical on the GNR surface (GCE/GNRs/diazo).

The latter GCE/GNRs/diazo modification was performed by click chemistry through the azide group and the alkyne group of the ethynylferrocene. This reaction was catalyzed by Cu(I) ions. To this end, the GCE/GNRs/diazo system was submerged in a solution containing a mixture of 4-ethynylferrocene (0.3 mM) in EtOH/H_2O (4:1), $CuSO_4$ (0.6 mM), and ascorbic acid (3 mM), during 18 h. After the incubation time, the resulting system, denoted as GCE/GNRs/diazo/Fc, was sonicated in EtOH/H_2O for 1 min to remove the ferrocene that was adsorbed but not covalently attached.

4.3.2.3. GCE/GNRs/diazo/Fc@β-CD: Supramolecular Interaction. Once the electrode was functionalized with the ferrocene group, the interaction with the supramolecular receptor was carried out by dipping the electrode into the corresponding solution (*β*-CD = 0.6 mM) for 18 h. The supramolecular complex formation was monitored by the decrease of the Fc electrochemical signal with time until it attained a constant minimum value. This procedure was also employed when other supramolecular receptors, such as CB[7] or CB[8], were evaluated.

The GCE/GNRs/diazo/Fc@*β*-CD surface was visualized by AFM. The samples for AFM and SEM measurements were prepared in the same way described above but by employing glassy carbon rod surfaces.

4.3.2.4. Electrochemical Measurements. The electrochemical measurements were performed with a three-electrode cell incorporating a GCE/GNRs/diazo/Fc@*β*-CD as a working electrode, a Ag/AgCl/KCl (3M) reference electrode, and a platinum wire as the counter electrode. Cyclic voltammetry (CV) measurements were recorded at 100 mV/s from −0.25 to 0.90 V, except for the diazotization procedure (CVs recorded at 200 mV/s from 0.10 to 1.0 V). Differential pulse voltammetry (DPV) measurements were carried out from 0.0 to 0.70 V in 0.1 M sodium perchlorate as the supporting electrolyte. The scan rate and the pulse amplitude employed were 30 and 90 mV, respectively.

4.3.2.5. Evaluation of the Sensor Response: Competitive Assay. The evaluation of the sensor response toward stigmasterol was performed by following the electrochemical signal of the ferrocene group, and it was based on the different affinity of the supramolecular receptor (CB[7], CB[8], or *β*-CD) for the redox probe (ferrocene) and the analyte (stigmasterol). The electrochemical response of the ferrocene group in the GCE/GNRs/diazo/Fc system was clearly diminished when the supramolecular complex between ferrocene and the corresponding supramolecular receptor was formed. After immersion of the sensor in a solution containing stigmasterol, a new complex between stigmasterol and the supramolecular receptor was formed, and the electrochemical signal of ferrocene clearly increased.

■ ASSOCIATED CONTENT

Supporting Information

The Supporting Information is available free of charge at https://pubs.acs.org/doi/10.1021/acsomega.4c06639.

(Figures S1, S2, and S3) Cyclic voltammograms, Nyquist plots, and SEM images of the different platforms resulting from each step of sensor construction, respectively; (Figure S4) AFM images of the GNR-modified electrode; (Table S1) optimal conditions for the sensor construction; (Table S2) comparison of the analytical properties of different stigmasterol determination methods (PDF)

https://doi.org/10.1021/acsomega.4c06639
ACS Omega 2024, 9, 39242−39252

AUTHOR INFORMATION

Corresponding Authors

Elena Casero − *Departamento de Química Analítica y Análisis Instrumental, Facultad de Ciencias, Campus de Excelencia de la Universidad Autónoma de Madrid, Madrid 28049, Spain*; Email: elena.casero@uam.es

Carmen Quintana − *Departamento de Química Analítica y Análisis Instrumental, Facultad de Ciencias, Campus de Excelencia de la Universidad Autónoma de Madrid, Madrid 28049, Spain*; orcid.org/0000-0002-3879-848X; Email: carmen.quintana@uam.es

Authors

Rut Martínez-Moro − *Departamento de Química Analítica y Análisis Instrumental, Facultad de Ciencias, Campus de Excelencia de la Universidad Autónoma de Madrid, Madrid 28049, Spain*

Luis Vázquez − *Instituto de Ciencia de Materiales de Madrid (ICMM), CSIC, Campus de Excelencia de la Universidad Autónoma de Madrid, Madrid 28049, Spain*; orcid.org/0000-0001-6220-2810

María Pérez − *Departamento de Química Analítica y Análisis Instrumental, Facultad de Ciencias, Campus de Excelencia de la Universidad Autónoma de Madrid, Madrid 28049, Spain*

María del Pozo − *Departamento de Química Analítica y Análisis Instrumental, Facultad de Ciencias, Campus de Excelencia de la Universidad Autónoma de Madrid, Madrid 28049, Spain*

Manuel Vilas-Varela − *Centro Singular de Investigación en Química Biolóxica e Materiais Moleculares (CIQUS) and Departamento de Química Orgánica, Universidade de Santiago de Compostela, Santiago de Compostela 15782, Spain*; orcid.org/0000-0002-6768-5441

Jesús Castro-Esteban − *Centro Singular de Investigación en Química Biolóxica e Materiais Moleculares (CIQUS) and Departamento de Química Orgánica, Universidade de Santiago de Compostela, Santiago de Compostela 15782, Spain*

M. Dolores Petit-Domínguez − *Departamento de Química Analítica y Análisis Instrumental, Facultad de Ciencias, Campus de Excelencia de la Universidad Autónoma de Madrid, Madrid 28049, Spain*

Complete contact information is available at: https://pubs.acs.org/10.1021/acsomega.4c06639

Notes

The authors declare no competing financial interest.

ACKNOWLEDGMENTS

The authors acknowledge financial support from projects PID2020-113142RB-C21, PID2020-113142RB-C22, PID2023-149077OB-C31, and PID2023-149077OB-C32 funded by MCIN/AEI/10.13039/501100011033 and P2018/NMT-4349 (TRANSNANOAVANSENS-CM) funded by the Comunidad Autónoma de Madrid. We want to thank I. Ballesteros for the SEM measurements.

REFERENCES

(1) Bianco, A.; Chen, Y.; Frackowiak, E.; Holzinger, M.; Koratkar, N.; Meunier, V.; Mikhailovsky, S.; Strano, M.; Tascon, J. M. D.; Terrones, M. Carbon science perspective in 2020: Current research and future challenges. *Carbon* **2020**, *161*, 373−391.

(2) Guan, X.; Li, Z.; Geng, X.; Lei, Z.; Karakoti, A.; Wu, T.; Kumar, P.; Yi, J.; Vinu, A. Emerging Trends of Carbon-Based Quantum Dots: Nanoarchitectonics and Applications. *Small* **2023**, *19*, 2207181.

(3) Bose, R.; Alanazi, A. K.; Bhowmik, S.; Garai, S.; Roy, M.; Pakhira, B.; Pramanik, T. Applications of Graphene and Graphene Oxide as Versatile Sensors: A Brief Review. *Biointerface Res. Appl. Chem.* **2023**, *13*, 457.

(4) Buffon, E.; Stradiotto, N. R. Disposable three-dimensional graphene oxide electrode with sandwich-like architecture for the determination of ascorbic acid in fruit juices. *Mater. Today Commun.* **2023**, *35*, No. 105535.

(5) Stozhko, N. Y.; Khamzina, E. I.; Bukharinova, M. A.; Tarasov, A. V. An Electrochemical Sensor Based on Carbon Paper Modified with Graphite Powder for Sensitive Determination of Sunset Yellow and Tartrazine in Drinks. *Sensors* **2022**, *22*, 4092.

(6) Tran, Q. T.; Phung, T. T.; Nguyen, Q. T.; Le, T. G.; Lagrost, C. Highly sensitive and rapid determination of sunset yellow in drinks using a low-cost carbon material-based electrochemical sensor. *Anal. Bioanal. Chem.* **2019**, *411*, 7539−7549.

(7) Malarat, N.; Oin, W.; Kanjana, K.; Makkliang, F.; Siaj, M.; Poorahong, S. Electrochemical platform based on activated carbon/graphene oxide-gold nanoparticle composites for the electrochemical sensing of methylparaben in cosmetic samples. *Microchem. J.* **2022**, *188*, No. 108473.

(8) Yue, X.; Li, Z.; Zhao, S. A new electrochemical sensor for simultaneous detection of sulfamethoxazole and trimethoprim antibiotics based on graphene and ZnO nanorods modified glassy carbon electrode. *Microchem. J.* **2020**, *159*, No. 105440.

(9) Mounesh; Manikanta, P.; Nikam, R. R.; Tigari, G.; Nagaraja, B. M. Novel nickel(II) phthalocyanine/reduced graphene oxide: an electrochemical sensing platform for analysis of hydroquinone and chloramphenicol in environmental samples. *Anal. Methods* **2024**, *16*, 1770−1784.

(10) Manikanta, P.; Mounesh; Nikam, R. R.; Sandeep, S.; Nagaraja, B. M. Development of novel microsphere structured − calcium tungstate as efficacious electrocatalyst for the detection of antibiotic drug nitrofurantoin. *J. Mater. Chem. B* **2023**, *11*, 11600.

(11) Mounesh; Reddy, K. R. V.; Pandith, A.; Eldesoky, G. E.; Nagaraja, B. M. Novel nitrogen-rich anchored nickel (II) phthalocyanine with composite of multiwalled carbon nanotubes on modified glassy carbon electrode: Sensitive and selective electrocatalytic activity of nitrite. *Appl. Organomet. Chem.* **2024**, *38*, No. e7302.

(12) Manikanta, P.; Mounesh; Nikam, R. R.; Mohanty, J.; Balakrishna, R. G.; Sandeep, S.; Nagaraja, B. M. CdO Decorated with Polypyrrole Nanotube Heterostructure: Potent Electrocatalyst for the Detection of Antihistamine Drug Promethazine Hydrochloride in Environmental Samples. *Langmuir* **2023**, *39*, 11099−11107.

(13) Mounesh; Yatish, K. V.; Pandith, A.; Eldesoky, G. E.; Nagaraja, B. M. A novel MWCNT-encapsulated (2-aminoethyl)piperazine-decorated zinc(II) phthalocyanine composite: development of an electrochemical sensor for detecting the antipsychotic drug promazine in environmental samples. *J. Mater. Chem. B* **2023**, *11*, 10692.

(14) Mounesh; Kumar, T. M. S.; Kumar, N. Y. P.; Reddy, K. R. V.; Chandrakala, K. B.; Arunkumar, L.; Vidyasagar, C. C. Novel Schiff base cobalt(II) phthalocyanine with appliance of MWCNTs on GCE: enhanced electrocatalytic activity behaviour of a-amino acids. *RSC Adv.* **2021**, *11*, 16736.

(15) Sainz, R.; del Pozo, M.; Vilas-Varela, M.; Castro-Esteban, J.; Pérez Corral, M.; Vázquez, L.; Blanco, E.; Peña, D.; Martín-Gago, J. A.; Ellis, G. J.; Petit-Domínguez, M. D.; Quintana, C.; Casero, E. Chemically synthesized chevron-like graphene nanoribbons for electrochemical sensors development: determination of epinephrine. *Sci. Rep.* **2020**, *10*, 14614.

(16) Tian, C.; Miao, W.; Zhao, L.; Wang, J. Graphene nanoribbons: Current status and challenges as quasi-one-dimensional nanomaterials. *Rev. Phys.* **2023**, *10*, No. 100082.

(17) Vo, T. H.; Shekhirev, M.; Kunkel, D. A.; Morton, M. D.; Berglund, E.; Kong, L.; Wilson, P. M.; Dowben, P. A.; Enders, A.;

Sinitskii, A. Large-scale solution synthesis of narrow graphene nanoribbons. *Nat. Commun.* **2014**, *5*, 1−8.
(18) Zhu, Y.; Higginbotham, A. L.; Tour, J. M. Covalent Functionalization of Surfactant-Wrapped Graphene Nanoribbons. *Chem. Mater.* **2009**, *21*, 5284−5291.
(19) Genorio, B.; Znidarsic, A. Functionalization of graphene nanoribbons. *J. Phys. D: Appl. Phys.* **2014**, *47*, No. 094012.
(20) Levrie, K.; Jans, K.; Vos, R.; Ardakanian, N.; Verellen, N.; Van Hoof, C.; Lagae, L.; Stakenborg, T. Multiplexed site-specific electrode functionalization for multitarget biosensors. *Bioelectrochemistry* **2016**, *112*, 61−66.
(21) Daukiya, L.; Teyssandier, J.; Eyley, S.; El Kazzi, S.; Rodríguez González, M. C.; Pradhan, B.; Thielemans, W.; Hofkens, J.; De Feyter, S. Covalent functionalization of molybdenum disulfide by chemically activated diazonium salts. *Nanoscale* **2021**, *13*, 2972.
(22) Strzemińska, I.; Sainte Rose Fanchine, S.; Anquetin, G.; Reisberg, S.; Noël, V.; Pham, M. C.; Piro, B. Grafting of a peptide probe for Prostate-Specific Antigen detection using diazonium electroreduction and click chemistry. *Biosens. Bioelectron.* **2016**, *81*, 131−137.
(23) Chen, G. Y.; Sun, Y. B.; Shi, P. C.; Liu, T.; Li, Z. H.; Luo, S. H.; Wang, X. C.; Cao, X. Y.; Ren, B.; Liu, G. K.; Yang, L. L.; Tian, Z. Q. Revealing unconventional host−guest complexation at nanostructured interface by surface-enhanced Raman spectroscopy. *Light Sci. Appl.* **2021**, *10*, 85.
(24) del Pozo, M.; Casero, E.; Quintana, C. Visual and spectrophotometric determination of cadaverine based on the use of gold nanoparticles capped with cucurbiturils or cyclodextrins. *Microchim. Acta* **2017**, *184*, 2107−2114.
(25) Ashwin, B. C. M. A.; Shanmugavelan, P.; Muthu Mareeswaran, P. Electrochemical aspects of cyclodextrin, calixarene and cucurbituril inclusion complexes. *J. Incl. Phenom. Macrocycl. Chem.* **2020**, *98*, 149−170.
(26) Wang, S. Y.; Li, L.; Xiao, Y.; Wang, Y. Recent advances in cyclodextrins-based chiral-recognizing platforms. *TrAC-. Trends Analyt Chem.* **2019**, *121*, No. 115691.
(27) Luo, H.; Chen, L.-X. X.; Ge, Q.-M. M.; Liu, M.; Tao, Z.; Zhou, Y.-H. H.; Cong, H. Applications of macrocyclic compounds for electrochemical sensors to improve selectivity and sensitivity. *J. Incl. Phenom. Macrocycl. Chem.* **2019**, *95*, 171−198.
(28) Barrow, S. J.; Kasera, S.; Rowland, M. J.; del Barrio, J.; Scherman, O. A. Cucurbituril-Based Molecular Recognition. *Chem. Rev.* **2015**, *115*, 12320−12406.
(29) Yang, L.; Zhao, H.; Fan, S.; Zhao, G.; Ran, X.; Li, C. P. Electrochemical detection of cholesterol based on competitive host−guest recognition using a β-cyclodextrin/poly(N -acetylaniline)/graphene-modified electrode. *RSC Adv.* **2015**, *5*, 64146−64155.
(30) Wang, M.; Huang, W.; Hu, Y.; Zhang, L.; Shao, Y.; Wang, M.; Zhang, F.; Zhao, Z.; Mei, X.; Li, T.; Wang, D.; Liang, Y.; Li, J.; Huang, Y.; Zhang, L.; Xu, T.; Song, H.; Zhong, Y.; Lu, B. Phytosterol Profiles of Common Foods and Estimated Natural Intake of Different Structures and Forms in China. *J. Agric. Food Chem.* **2018**, *66*, 2669−2676.
(31) Ramprasath, V. R.; Awad, A. B. Role of Phytosterols in Cancer Prevention and Treatment. *J. AOAC Int.* **2015**, *98*, 735.
(32) Khairi, N. A. S.; Yusof, N. A.; Abdullah, J.; Seman, I. A.; Ithnin, N.; Abd Rahman, S. F. β-Cyclodextrin Functionalized Reduced Graphene Oxide-Gold Nanoparticles for Electrochemical Detection of Stigmasterol in Ganoderma boninense-Infected Oil Palm Leaves. *IEEE Sens J.* **2024**, *24*, 9341−9352.
(33) Santanatoglia, A.; Nzekoue, F. K.; Sagratini, G.; Ricciutelli, M.; Vittori, S.; Caprioli, G. Development and application of a novel analytical method for the determination of 8 plant sterols/stanols in 22 legumes samples. *Journal of Food Composition and Analysis* **2023**, *118*, No. 105195.
(34) Özdemir, İ. S.; Dağ, C.; Özinanç, C.; Suçsoran, O.; Ertaş, E.; Bekiroğlu, S. Quantification of sterols and fatty acids of extra virgin olive oils by FT-NIR spectroscopy and multivariate statistical analyses. *LWT* **2018**, *91*, 125−132.
(35) Zhang, J. J.; Gao, Y.; Xu, X.; Zhao, M. L.; Xi, B. N.; Shu, Y.; Li, C.; Shen, Y. In Situ Rapid Analysis of Squalene, Tocopherols, and Sterols in Walnut Oils Based on Supercritical Fluid Chromatography-Quadrupole Time-of-Flight Mass Spectrometry. *J. Agric. Food Chem.* **2023**, *71*, 16371−16380.
(36) Nandhini, N. S.; Llango, K. Simultaneous Quantification of Lupeol, Stigmasterol and β- Sitosterol in Extracts of Adhatoda vasica Nees Leaves and its Marketed Formulations by a Validated RP-HPLC Method. *Pharmacogn. J.* **2020**, *12*, 850−856.
(37) Kolarič, L.; Šimko, P. Simultaneous determination of cholesterol, stigmasterol, and β-sitosterol contents in milk and dairy products. *J. Food Process Preserv* **2022**, *46*, No. e16146.
(38) Fagundes, M. B.; Alvarez-Rivera, G.; Vendruscolo, R. G.; Voss, M.; da Silva, P. A.; Barin, J. S.; Jacob-Lopes, E.; Zepka, L. Q.; Wagner, R. Green microsaponification-based method for gas chromatography determination of sterol and squalene in cyanobacterial biomass. *Talanta* **2021**, *224* (2021), No. 121793.
(39) Lee, J.; Weon, J. B.; Yun, B. R.; Eom, M. R.; Ma, C. J. Simultaneous determination three phytosterol compounds, campesterol, stigmasterol and daucosterol in Artemisia apiacea by high performance liquid chromatography-diode array ultraviolet/visible detector. *Pharmacogn Mag.* **2015**, *11*, 297.
(40) Shekhirev, M.; Vo, T. H.; Kunkel, D. A.; Lipatov, A.; Enders, A.; Sinitskii, A. Aggregation of atomically precise graphene nanoribbons. *RSC Adv.* **2017**, *7*, 54491−54499.
(41) Sainz, R.; del Pozo, M.; Vázquez, L.; Vilas-Varela, M.; Castro-Esteban, J.; Blanco, E.; Petit-Domínguez, M. D.; Quintana, C.; Casero, E. Lactate biosensing based on covalent immobilization of lactate oxidase onto chevron-like graphene nanoribbons via diazotization-coupling reaction. *Anal. Chim. Acta* **2022**, *1208*, No. 339851.
(42) Evrard, D.; Lambert, F.; Policar, C.; Balland, V.; Limoges, B. Electrochemical Functionalization of Carbon Surfaces by aromatic Azide or Alkyne Molecules: A versatile platform for click chemistry. *Chem. - Eur. J.* **2008**, *14*, 9286−9291.
(43) Yeap, W. S.; Murib, M. S.; Cuypers, W.; Liu, X.; van Grinsven, B.; Ameloot, M.; Fahlman, M.; Wagner, P.; Maes, W.; Haenen, K. Boron-Doped Diamond Functionalization by an Electrografting/Alkyne−Azide Click Chemistry Sequence. *ChemElectroChem.* **2014**, *1*, 1145−1154.
(44) Brooksby, P. A.; Downard, A. J. Electrochemical and atomic force microscopy study of carbon surface modification via diazonium reduction in aqueous and acetonitrile solutions. *Langmuir* **2004**, *20*, 5038−5045.
(45) Greenwood, J.; Phan, T. H.; Fujita, Y.; Li, Z.; Ivasenko, O.; Vanderlinden, W.; Van Gorp, H.; Frederickx, W.; Lu, G.; Tahara, K.; Tobe, Y.; Uji-I, H.; Mertens, S. F. L.; De Feyter, S. Covalent modification of graphene and graphite using diazonium chemistry: tunable grafting and nanomanipulation. *ACS Nano* **2015**, *9*, 5520−5535.
(46) González, M. C. R.; Carro, P.; Vázquez, L.; Creus, A. H. Mapping nanometric electronic property changes induced by an aryl diazonium sub-monolayer on Hopg. *Phys. Chem. Chem. Phys.* **2016**, *18*, 29218−29225.
(47) He, Y.; Fu, P.; Shen, X.; Gao, H. Cyclodextrin-based aggregates and characterization by microscopy. *Micron* **2008**, *39*, 495−516.

https://doi.org/10.1021/acsomega.4c06639
ACS Omega 2024, 9, 39242−39252